EFFECTS OF ADVERSE PRESSURE GRADIENT ON A TURBULENT BOUNDARY LAYER

Joung-Ho Lee
Department of Mechanical Engineering,
Korea Advanced Institute of Science and Technology,
373-1, Guseong-dong, Yuseong-gu, Daejeon, 305-701, Korea
leejh34@kaist.ac.kr

Hyung Jin Sung
Department of Mechanical Engineering,
Korea Advanced Institute of Science and Technology,
373-1, Guseong-dong, Yuseong-gu, Daejeon, 305-701, Korea
hjsung@kaist.ac.kr

ABSTRACT

Direct numerical simulations were performed to investigate the physics of turbulent boundary layer flows subjected to adverse pressure gradient. A fully implicit fractional step method was employed to simulate the flows. To avoid generating an inflow with adverse pressure gradient, the sufficient streamwise length was placed from the inlet to the sudden change of free-stream velocity. The spatially-developing characteristics of turbulent boundary layer with adverse pressure gradient were examined. The present results were in good agreement with previous experimental ones. The visualization results showed that the adverse pressure gradient weakens the vortical structures. This causes a reduction in turbulence intensity near the wall.

NOMENCLATURE

C_p = Pressure coefficient, normalized by the inlet free-stream velocity, U_0

G = Shape factor,
$= \frac{1}{\Delta}\int_0^\infty \left((U-u)/u_\tau\right)^2 dy$

P = Mean pressure

P^+ = $\nu(dP/dx)/\rho u_\tau^3$

β = Clauser pressure gradient parameter,
$= (\delta^*/\tau_w)dP/dx$

Δ = Defect thickness
$= \int_0^\infty (U-u)/u_\tau dy$

θ_{in} = Inlet momentum thickness

INTRODUCTION

Turbulent boundary layers with adverse pressure gradient are found in many engineering applications including diffusers, turbine blades and the trailing edges of airfoils *etc*. It is of both fundamental and practical significance to understand the structure of turbulent boundary layer affected by adverse pressure gradient. Clauser (1954) suggested a new class of the equilibrium boundary layer with adverse pressure gradient, where the profiles of velocity-defect and of turbulent stresses at different streamwise stations show a similarity when properly scaled. Following Clauser, a number of theoretical and experimental studies on adverse pressure gradient flows were made throughout the past decades. However, the physics of adverse pressure gradient flows and the interaction with turbulence and structures are not fully understood.

In the present study, we simulated a spatially developing turbulent boundary layer with adverse pressure gradient using direct numerical simulation in order to elucidate the effect on the near-wall and outer layer turbulent structures of adverse pressure gradient. First the numerical method is described briefly and some results are compared with the flows with zero pressure gradient.

NUMERICAL METHODS

Direct numerical simulations are performed to investigate the physics of spatially developing turbulent boundary layer flows subjected to adverse pressure gradient. A schematic diagram of the computational domain is displayed in Fig. 1. Time-dependent zero pressure gradient turbulent inflow data are provided at the inlet based on the method of Lund *et al.* (1998). A convective boundary condition at the exit has the form $(\partial u/\partial t)+c(\partial u/\partial x)=0$, where c is the local bulk velocity. The no-slip condition is imposed at the solid wall. Periodic boundary conditions are applied in the spanwise direction. Townsend (1961) and Mellor & Gibson (1966) showed that an approximate equilibrium flow is obtained when the variation of free-stream has the form of a power-law relation in the streamwise direction. A free-stream velocity $U_\infty(x)$ along the upper boundary of the computational domain is prescribed as,

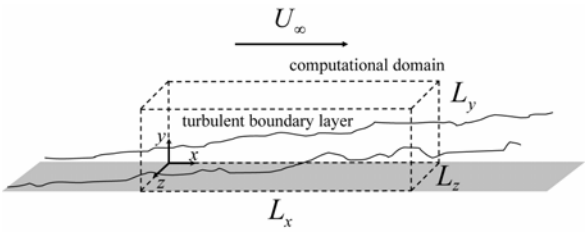

Fig. 1: Schematic diagram of computational domain.

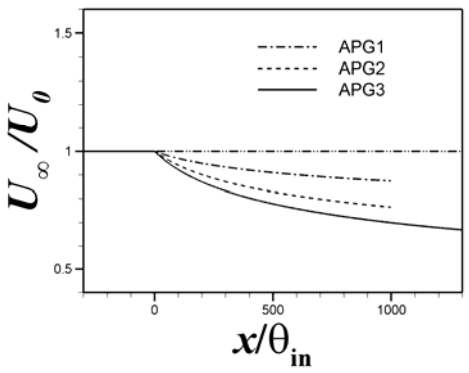

Fig. 2: Free-stream velocity distributions along the upper boundary of computational domain.

Table 1: Case parameters

Designation	m	x_0	Re_θ
ZPG	0	∞	1410
APG1	-0.075	-200	750 ~ 1000
APG2	-0.150	-200	770 ~ 1035
APG3	-0.200	-200	1125 ~ 1290

$$U_\infty(x) = U_0\left(1 - \frac{x}{x_0}\right)^m ,$$

where m denotes the exponent of adverse pressure gradient (Fig. 2). Four cases are considered, defined by the exponent of adverse pressure gradient summarized in Table 1. Since adverse pressure gradient flows are very sensitive to upstream conditions, sufficient streamwise length from the inlet to the sudden change of free-stream velocity is required to obtain an equilibrium flow.

Our method simulates without any assumptions on the evolution of boundary layer and no extra terms are added to the Navier-Stokes equations. The Navier-Stokes equations are integrated in time using the fractional step method with

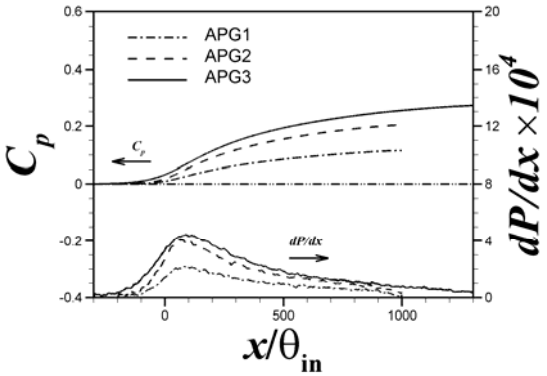

Fig. 3: Mean wall-pressure coefficient based on free-stream velocity at inlet.

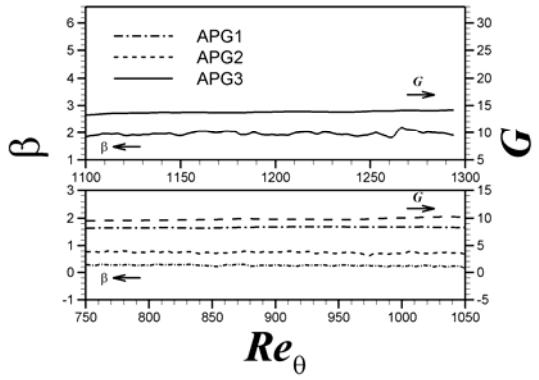

Fig. 4: Clauser's equilibrium parameter: non-dimensionalized pressure gradient parameter, β, shape factor G.

Table 2: Mean flow parameters

Designation	m	β	G
APG1	-0.075	0.26	8.33
APG2	-0.150	0.74	9.85
APG3	-0.200	1.97	13.8

an implicit velocity decoupling procedure proposed by Kim *et al.* (2002). All the terms are discretized with Crank-Nicolson method in time, the coupled velocity components in the convection term are decoupled by the implicit velocity decoupling procedure. The decoupled velocity components are solved without iteration. Since the implicit decoupling procedure relieves the CFL restriction, the computation time is significantly reduced. The mesh is uniform in the streamwise and spanwise directions. However a hyperbolic tangent distribution is used in the wall-normal direction. The mesh resolutions are $\Delta x^+ = 12.5$, $\Delta y^+_{\min} = 0.17$, $\Delta y^+_{MAX} = 24$ and $\Delta z^+ = 5$ based on the friction velocity at the inlet. The computational time step used is $\Delta t^+ = 0.25$.

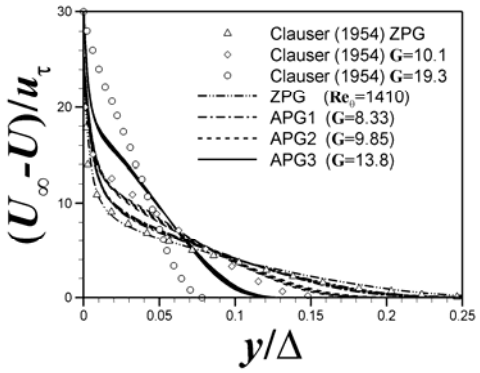

Fig. 5: Mean velocity profiles for five positions downstream in the equilibrium region.

RESULTS AND DISCUSSION

Mean pressure gradient

The streamwise distributions of wall-pressure coefficient and wall-pressure gradient are shown in Fig. 3. It is seen that the boundary layer develops under a zero pressure gradient at the inlet and then the streamwise pressure gradient becomes strongly adverse. After the inflection point, pressure gradient decreases slowly. On the other hand, Clauser pressure gradient parameter increases and then keeps a nearly constant. Throughout the rest of this paper we shall call this constant Clauser pressure gradient region 'equilibrium region'. Table 2 lists Clauser's parameters in the equilibrium region for three adverse pressure flows considered here.

Mean velocity and turbulent intensities

Figure 5 shows the velocity defect profiles at various locations along the streamwise direction in the equilibrium region. The velocity profiles are normalized by the friction velocity u_τ and defect thickness Δ. The velocity defect profiles almost collapse, indicating that the outer-layer similarity is established in this region. As seen in Fig. 4 the Clauser's equilibrium parameter β varies little and G is almost constant. Thus we can conclude that the simulations fulfill the requirements of self-similarity well.

Evolutions of the mean velocity in the non-equilibrium region of APG3 are shown in Fig. 6 (a). The law of the wall $U^+ = y^+$ holds in the viscous sublayer ($y^+ < 5$). The velocity profiles are shifted downward monotonically with increasing Clauser pressure gradient and the wake occupies an increasing fraction of the boundary thickness as the flow moves downstream. This characteristic of the non-equilibrium APG flows is confirmed by the experiments of Nagano and Houra (2002). However the slope in the log region is changed unlike Nagano *et al.* (1997) whose the velocity profiles deviate downwards without change in

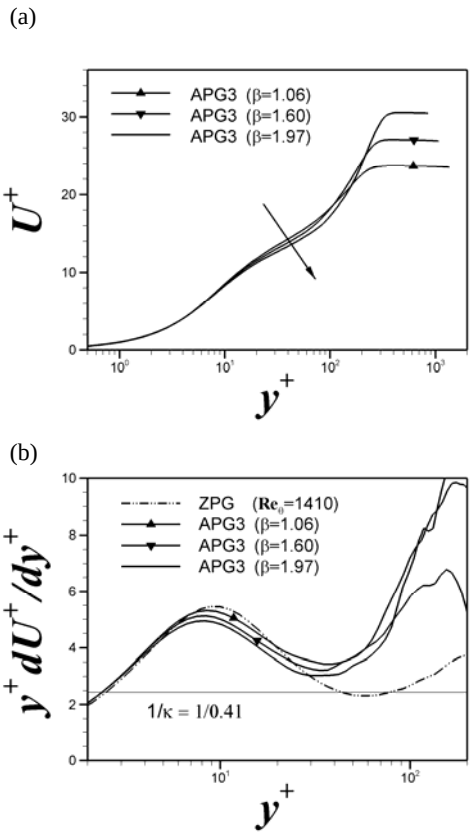

Fig. 6: Mean velocity profiles in the non-equilibirium region.

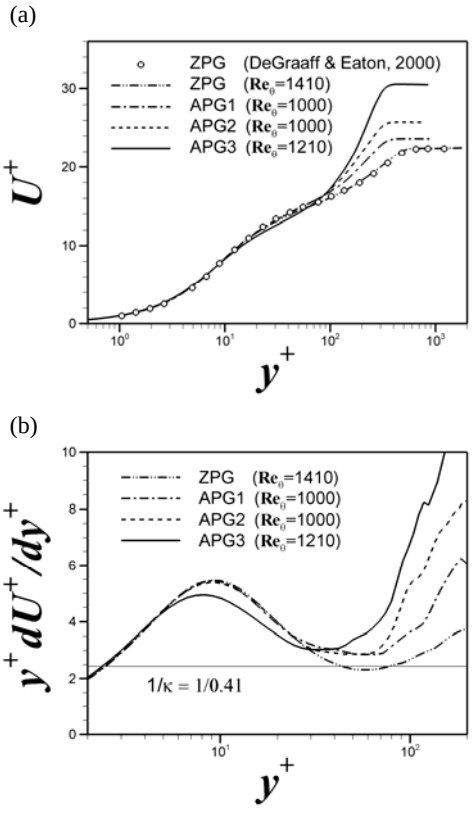

Fig. 7: Mean velocity profiles in the equilibrium region.

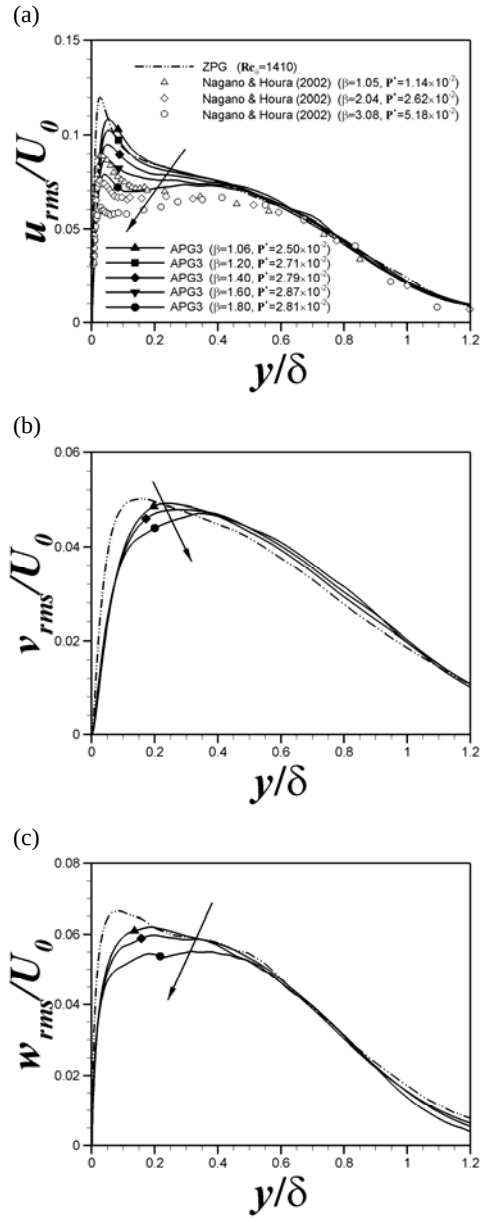

Fig. 8: Root-mean-square velocity fluctations in the non-equilibrium region.

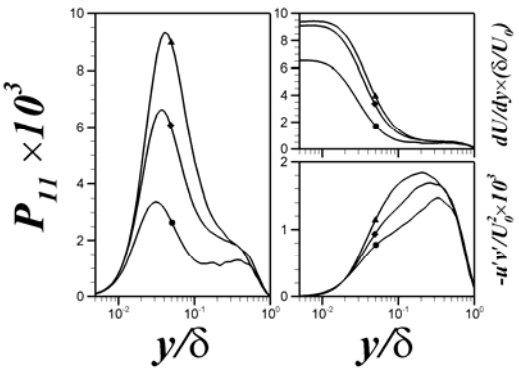

Fig. 9: Production term of u_{rms}. For symbols see Fig. 8.

slope (Fig. 6 (b)). The starting point of the logarithmic law is lower than that of zero pressure gradient ($y^+ \approx 30$). Some of this difference may be owing to the low Reynolds number and the effect of increasing wake region.

The logarithmic velocity profiles in the equilibrium region are plotted in Fig. 7 (a). The zero pressure gradient flows of DeGraaff & Eaton (2000) and our calculation are shown for comparison. Krogstad & Skåre (1994) suggested that adverse pressure gradient did not influence the law of the wall with von Kármán constant $\kappa = 0.41$. For weak adverse pressure gradient (APG1 & APG2), inner layer mean velocity profiles are in good agreement with that of the zero pressure gradient flow. For APG3, however, the velocity profiles are shifted downward slightly in the log region. Similar discrepancy is seen in the low Reynolds number DNS of Skote *et al.* (1998). The variations of $y^+ dU^+/dy^+$ are compared in Fig. 7 (b). This presents that the slopes in the log region are almost the same for the three different pressure gradient equilibrium flows. However the value of slope is higher than that of zero pressure gradient flow.

Figure 8 shows the root-mean-square (rms) velocity fluctuations in the non-equilibrium region along with the data of Nagano & Houra (2002). The profiles of fluctuating quantities are normalized by the inlet free-stream velocity and boundary thickness. It is clear from Fig. 8 that the all calculated velocity fluctuations in the inner region decrease with increasing β. These trends are in good agreement with the experimental data. Many previous experimental and numerical studies have found that turbulent intensities are reduced in the inner layer (Nagano & Houra and Coleman *et al.* (2003)). For u_{rms}, the reduction in the inner layer is mainly due to the decrease of the production term, $P_{11} \approx -2u'v'(dU/dy)$, which is the dominant source of u_{rms}. The mean shear dU/dy is significantly reduced with increasing β. This leads to the decreasing inner maximum peak of the production term as seen in Fig. 9. For higher β, the *y*-locations for the local maximum of Reynolds shear stress move outward and the mean shear is almost constant in the outer layer. Hence, the second peak appears in the profiles of P_{11} around at $y/\delta \approx 0.4$. This promotes that the second peak appears roughly at $y/\delta \approx 0.4$ in the profiles of u_{rms}. This second peak has been observed in many previous studies, such as Nagano & Houra and Korgstad & Skåre.

In the outer layer $y/\delta > 0.5$, the rms velocities of streamwise and spanwise components (u_{rms}, w_{rms}) are similar and identical with those of zero pressure gradient flows. The behaviour of the wall-normal velocity fluctuations v_{rms} is slightly different from the other components. The wall-normal velocity fluctuations are higher than those of zero pressure gradient flows and increase monotonically with increasing β. Coleman *et al.* (2003) show that the variation of v_{rms} respond in the outer layer.

Root-mean-square pressure fluctuations as a function of wall-normal distance are shown in Fig. 10. Initially, pressure fluctuation profiles have one local maximum at

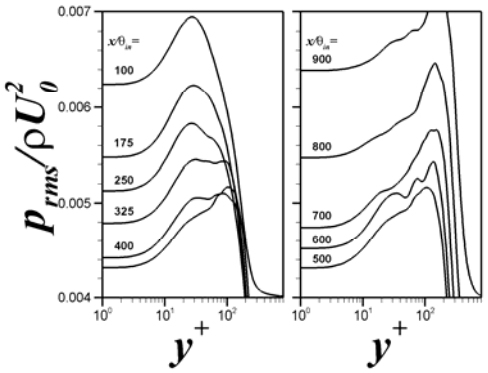

Fig. 10: Root-mean-square pressure fluctuations

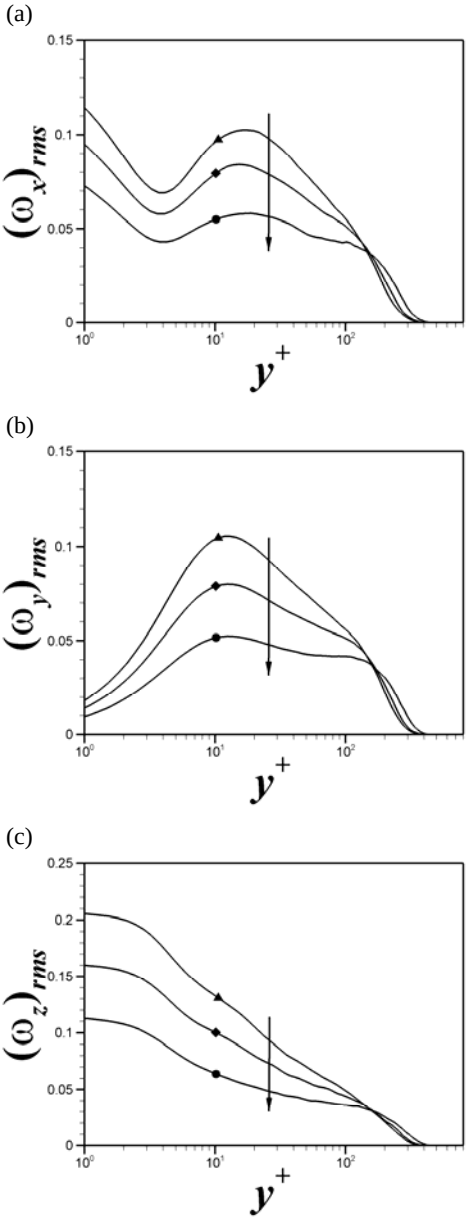

Fig. 11: Root-mean-square vorticity fluctations in the non-equilibrium region. For symbols see Fig. 8.

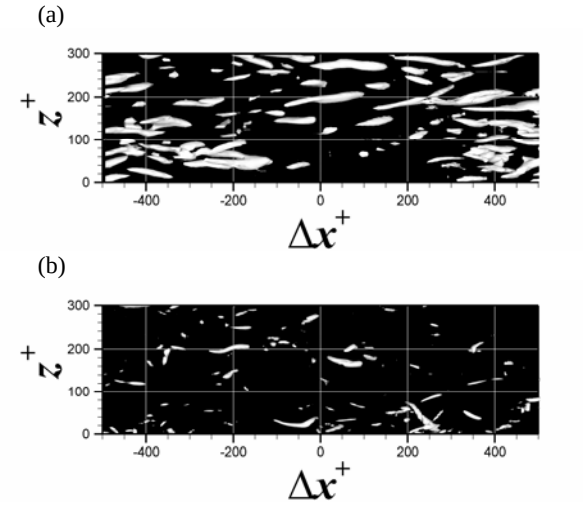

Fig. 12: Near wall streamwise vortex structures: isosurfaces of $\lambda_2 = -0.01$ (a) $\beta = 0$, (b) $\beta = 1.8$.

$y^+ \approx 30$. As flow moves downstream, the rms pressure fluctuations have an outer peak and the outer peak becomes more dominant than the inner peak for higher pressure gradient.

Turbulent vortical structures

The dominant structures in the near-wall region can be found by looking at the streamwise vortices. Figure 11 illustrates the rms vorticity fluctuations in the non-equilibrium region. Like the velocity fluctuations in Fig. 8, all the components of vorticity fluctuations are significantly decreased in the inner layer. Decrease of the streamwise and transverse vorticity fluctuations indicates weakened near-wall vortex and streaky structures respectively. The y -locations for the local maximum, which corresonds to the average location of the center of the streamwise vortices, are unchanged.

In order to observe the responses of the streamwise vortices to the adverse pressure gradient, the near-wall vortical structures are visualized using isosurfaces of λ_2 in Fig. 12 (Jeong & Hussain, 1995). In the adverse pressure gradient flow the streamwise vortical structures are significantly weaker than those of zero pressure gradient flow. It is known that near-wall vortical structures are closely related with the production of Reynolds shear stress (Robinson, 1991). The reduction of Reynolds shear stress is likely in part due to the weakening of streamwise vortices.

SUMMARY AND CONCLUSION

DNS of spatially developing turbulent boundary layer flows with adverse pressure gradients has been used to examine the effects of pressure gradient on turbulence statistics and near-wall structures. The characteristics of mean and rms quantities are in fair agreement with the Nagano & Houra's experimental data. The streamwise

vortex structures are weakened and the mean shear near the wall decreases by imposing adverse pressure gradient, which in turn leads to a reduction of Reynolds shear stress and turbulent intensity near the wall.

ACKNOWLEDGEMENTS

The authors would like to acknowledge the support from the Korea Institute of Science and Technology Information under the Grand Challenge Supercomputing Program.

REFERENCES

Clauser, F. H., 1954, "Turbulent boundary layers in adverse pressure gradients," Journal of the Aeronautical Science, Vol. 21, pp. 91-108.

Coleman, G. N., Kim, J. and Spalart, P. R., 2003, "Direct numerical simulation of a decelerated wall-bounded turbulent shear flow," Journal of Fluid Mechanics, Vol. 495, pp. 1-38.

DeGraaff, D. B. and Eaton, J. K., 2000, "Reynolds-number scaling of the flat-plate turbulent boundary layer," Journal of Fluid Mechanics, Vol. 422, pp. 319-346.

Houra, T., Tsuji, T. and Nagano, Y., 2000, "Effects of adverse pressure gradient on quasi-coherent structures in turbulent boundary layer," International Journal of Heat and Fluid Flow, Vol. 21, pp. 304-311.

Jeong, J. and Hussain, F., 1995, "On the identification of a vortex," Journal of Fluid Mechanics, Vol. 285, pp. 69-94.

Kim, K., Baek, S.-J. and Sung, H. J., 2002, "An implicit velocity decoupling procedure for the incompressible Navier-Stokes equations," International Journal of Numerical Methods in Fluids, Vol. 38, pp. 125-138.

Krogstad, P.-Å and Skåre, P. E., 1994, "A turbulent equilibrium boundary layer near separation," Journal of Fluid Mechanics, Vol. 272, pp.319-348.

Lund, T. S., Wu, X. and Squires, K. D., 1998, "Generation of turbulent inflow data for spatially-developing boundary layer simulations," Journal of Computational Physics, Vol. 140, pp.233-258.

Mellor, G. L. and Gibson, D. M., 1966, "Equilibrium turbulent boundary layers," Journal of Fluid Mechanics, Vol. 24, pp.225-253.

Nagano, Y. and Houra, T., 2002, "Higher-order moments and spectra of velocity fluctuations in adverse-pressre-gradient turbulent boundary layer," Experiments in Fluids, Vol. 33, pp. 22-30.

Nagano, Y., Tsuji, T. and Houra, T., 1997, "Structure of turbulent boundary layer subjected to adverse pressure gradient," Eleventhth Symposium on Turbulent Shear Flows, Grenoble, France, September 8-10, 1997.

Robinson, S. K., 1991, "Coherent motions in the turbulent boundary layer," Annual Review of Fluid Mechanics, Vol.23, pp. 601-639.

Skote, M., Henningson, D. S. and Henkes, R. A. W. M., 1998, "Direct numerical simulation of self-similar turbulent boundary laysers in adverse pressure gradients," Flow, Turbulence and Combustion, Vol. 60, pp. 47-85.

Townsend, A. A., 1961, "Equilibrium layers and wall turbulence," Journal of Fluid Mechanics, Vol. 11, pp. 97-120.